Mechatronics 35 (2016) 162–172

Contents lists available at ScienceDirect

Mechatronics

journal homepage: www.elsevier.com/locate/mechatronics

Simplified torque modulated microstepping for position control of permanent magnet stepper motors

Wonhee Kim[a], Donghoon Shin[b], Youngwoo Lee[b], Chung Choo Chung[c,*]

[a] School of Energy Systems Engineering, Chung-Ang University, Seoul 156-756, Republic of Korea
[b] Department of Electrical Engineering, Hanyang University, Seoul 133-791, Republic of Korea
[c] Division of Electrical and Biomedical Engineering, Hanyang University, Seoul 133-791, Republic of Korea

ARTICLE INFO

Article history:
Received 4 September 2015
Revised 25 January 2016
Accepted 12 February 2016
Available online 21 March 2016

Keywords:
Permanent magnet stepper motor
Position control
Singularly perturbed system

ABSTRACT

In previous methods designed based on field oriented (and/or weakening) control, high performance of current control is required for position control of permanent magnet (PM) stepper motors. This paper proposes a simplified torque modulated microstepping (STMMS) based on singular perturbation theory for position control of the PM stepper motors. Since a two phase frame PM stepper motor model involves slow and fast dynamics, singular perturbation theory is applied to improve the transient response and to reduce the ripple. The torque modulated microstepping method is applied with a simplified current tracking control law obtained from singular perturbed system analysis. Using applied conditions and stability proofs, we find that the proposed control design procedure is simplified. This eliminates the high-bandwidth control efforts for the current tracking required in the previous methods. Furthermore, the STMMS does not use current feedback for the current tracking. It is shown that high performance in the current tracking does not necessarily entail high performance in the position tracking. The proposed method was validated by simulation and experimental results. It is observed that the STMMS not only improved transient response but also reduced ripple in position control over the previous method. Furthermore, the STMMS used the input voltages less than the previous method does.

1. Introduction

Permanent magnet (PM) stepper motors have been widely used in positioning applications due to their durability, high efficiency, and power density as well as their high torque to inertia ratio and absence of rotor winding [1]. Their other merit is that PM stepper motors can be operated in open-loop control (i.e. full stepping or half stepping) [2]. However, PM stepper motors have a specific problem when used for precise positioning. Standard PM stepper motors have relatively large step sizes, usually $\frac{1}{200}$ of a revolution or 1.8°. Such large step sizes may cause motor-shaft oscillations at low speeds [3]. Microstepping has been widely used for improved resolution and significantly increased motion stability [4,5]. However, if microstepping is used to track the desired position trajectory in open-loop control, the currents of the PM stepper motor decrease due to back-emfs and have the phase lags. The degradation of the current tracking results in that of the position tracking in PM stepper motor. Thus, at least, the current regulation should be required in microstepping. Current feedback is generally obtained by the current sensor embedded in motor drive, so that proportional-integral controller is widely used in industrial applications [6,7]. Hysteresis current-control method was also used since it was simple to implement and has robust current control performance against load and source parameter changes [8]. Moreover, resolvers or encoders built into PM stepper motors are widely used for position feedback in industrial applications [9–12]. Recently, several feedback control methods were proposed to improve the position tracking performance of microstepping [13–16]. However, microstepping based control method with only current regulation has been limited by position tracking error that occurs during the nonzero velocity period since the electrical dynamics are much faster than the mechanical dynamics in PM stepper motor [17].

With the increase in power and decrease in cost of embedded processors in recent years, drives and control systems for PM stepper motor have become increasingly sophisticated. Thus, for positioning applications, PM stepper motor can be substituted for

* Corresponding author. Tel.: +82 2 2220 1724; fax: +82 2 2291 5307.
E-mail addresses: whkim79@cau.ac.kr (W. Kim), shin211@hanyang.ac.kr (D. Shin), stork@hanyang.ac.kr (Y. Lee), cchung@hanyang.ac.kr (C.C. Chung).

http://dx.doi.org/10.1016/j.mechatronics.2016.02.002
0957-4158/

Nomenclature

θ:	Rotor (angular) position [rad]
ω:	Rotor (angular) velocity [rad/s]
i_a, i_b:	Currents [A] of phases A and B
v_a, v_b:	Voltages [V] of phases A and B
B:	Viscous friction coefficient [N·m·s/rad]
J:	Inertia of the motor [Kg·m^2]
K_m:	Motor torque constant [N·m/A]
R:	Resistance of the phase winding [Ω]
L:	Inductance of the phase winding [H]
N_r:	Number of rotor teeth
τ_l:	Load torque [N·m]
V_s:	Supply voltage of PM stepper motor [V]
i_d, v_d:	Direct current [A] and voltage [V]
i_q, v_q:	Quadrature current [A] and voltage [V]
θ_d:	Desired rotor (angular) position [rad]
i_{a_d}, i_{b_d}:	Desired currents [A] of phases A and B

expensive servo motors such as PM synchronous motors as a cheaper replacement in closed-loop operation [18]. In order to improve the position (or velocity) tracking performance, various control methods [19–30] based on vector control with direct quadrature (DQ) transformation [31] have been studied. Since these previous methods were designed based on field oriented control (FOC) and/or field weakening control (FWC), high performance of current control is required for position control of PM stepper motors. Generally since using DQ transformation gives us the merit that PM stepper motor can be easily interpreted as direct current (DC) motor, the previous methods used DQ transformation so that their performances were analyzed in the view point of DC motor. Using DQ transformation removes sine and cosine functions in the PM stepper motor dynamics so that PM stepper motor dynamics becomes simple. Thus the stiff electrical dynamics become embedded and thus disappear in the PM stepper motor dynamics since using DQ transformation removes high frequency elements in the PM stepper motor dynamics. Therefore, there has been no study of the effect of high frequency elements on the position tracking performance. Although after DQ transformation, high frequency elements in the PM stepper motor dynamics are removed, this does not mean that high frequency elements are actually removed in the PM stepper motor. Hence a study of the effect of the high frequency elements on the position control is required. Recently, several methods based on microstepping without DQ transformations were studied to improve the position tracking performance of PM stepper motor [32,33]. FOC and FWC were designed in the view point of two phase frame. However, there was also no study of the effect of high frequency elements on the position control in [32,33].

Although all of those methods improved the position tracking performance of PM stepper motor, there is still a main problem in the position control. In PM stepper motor, the currents generated by the input voltages make the torque. Then, the generated torque makes the position track the desired position. Therefore, high performance in the current tracking is important for high performance in the position tracking control in the previous methods. The previous methods were designed based on cascade control concept and consist of position and current controllers. In the position control for PM stepper motor, since the current tracking of the electrical dynamics requires much wider bandwidth than the position tracking of the mechanical dynamics, the previous methods were designed to maintain wide bandwidth for the current tracking in the position tracking. Therefore, the control gain in the current controller was much higher than that in position controller [19–30,32,33]. Actually, in the PM stepper motor, the available input to track both desired currents and position is bounded. The high-bandwidth control effort for the desired currents with high frequencies may require the significant portion of whole available input. It may cause the limitation of increasing the control gain in the position controller since the control effort for the current tracking may saturate the input voltages in the PM stepper motor. Consequently, the position tracking performance may be degraded so that large overshoots and large ripples may appear. Furthermore, although the currents converge to the desired currents, it takes time for the position to converge to the desired position since the mechanical dynamics is much slower than the electrical dynamics.

Since the dynamics of PM stepper motor involves the slow dynamics (the mechanical dynamics) and the fast dynamics (the electrical dynamics), singular perturbation theory [34–36] can be applied to the position tracking control of a PM stepper motor. This would give us the simplification of the control design and reduction of the control efforts. However, application of the theory for PM stepper motor position control is rare. In [34,35] singular perturbation theory was applied for position control of DC motor. In [36], singular perturbation theory with DQ transformation was applied to reduce PM stepper motor model. There is no analysis of effects of both high frequency elements and wide bandwidth control effort for the current tracking to the position tracking performance in [34–36].

In this paper, we innovate an approach to position control, simplified torque modulated microstepping (STMMS), based on singular perturbation theory in order to resolve the problem of previous methods. The main contribution of this paper is the novel position control design to achieve the improved position tracking performance without the wide bandwidth control efforts for high performance in the current tracking based on singular perturbed system problem. We analyze the effect of high frequency elements on the position control. Singular perturbation theory is applied to the position tracking control of a PM stepper motor for solving the degradation problem of the position tracking performance due to the effect of high frequency elements. Singular perturbation theory shows that the negative feedback term using the current feedback is not necessary since the passive term is enough for the current tracking in the faster electrical dynamics. Thus, the wide bandwidth control effort for the current tracking is eliminated. Consequently, the significant portion of whole available input can be used for the position tracking instead of the current tracking so that the large position control gain can be utilized. The improved transient response and reduced ripples in the position control are achieved by the STMMS. It is shown that the high performance in the current tracking does not necessarily entail the high performance in the position tracking. The performance of the STMMS was validated via simulations and experiments. There were no overshoots in the position control during acceleration and deceleration periods and the position ripple was reduced by the STMMS compared to the previous method [32]. The STMMS used the input voltages less than the previous method.

2. System model of PM stepper motor and its analysis

In this paper, the modeling and the controller design will be studied based on the hybrid type PM stepper motor with 1.8° of angular resolution [1]. A hybrid type PM stepper motor consists of a slotted stator with two phases and a permanent magnet rotor which has north and south poles. Detailed descriptions of the operation of PM stepper motors are given in [23,37].

The dynamics of a PM stepper motor can be represented in the state-space form as follows [20,23,37]:

$$\begin{aligned}\dot{\theta} &= \omega \\ \dot{\omega} &= \frac{1}{J}[-K_m i_a \sin(N_r\theta) + K_m i_b \cos(N_r\theta) - B\omega - \tau_l] \\ \dot{i}_a &= \frac{1}{L}[v_a - Ri_a + K_m\omega \sin(N_r\theta)] \\ \dot{i}_b &= \frac{1}{L}[v_b - Ri_b - K_m\omega \cos(N_r\theta)]\end{aligned} \tag{1}$$

where θ is the rotor (angular) position [rad], ω is the rotor (angular) velocity [rad/s], and i_a, i_b and v_a, v_b are currents [A] and the voltages [V] of phases A and B, respectively. The dynamics of θ and ω are the mechanical dynamics, and the dynamics of i_a and i_b are the electrical dynamics.

The high frequency elements exist in the PM stepper motor dynamics (1). In order to remove the high frequency elements in PM stepper motor dynamics (1), various control methods used DQ transformation as defined by

$$\begin{bmatrix} i_d \\ i_q \end{bmatrix} = \begin{bmatrix} \cos(N_r\theta) & \sin(N_r\theta) \\ -\sin(N_r\theta) & \cos(N_r\theta) \end{bmatrix} \begin{bmatrix} i_a \\ i_b \end{bmatrix} \\ \begin{bmatrix} v_d \\ v_q \end{bmatrix} = \begin{bmatrix} \cos(N_r\theta) & \sin(N_r\theta) \\ -\sin(N_r\theta) & \cos(N_r\theta) \end{bmatrix} \begin{bmatrix} v_a \\ v_b \end{bmatrix} \tag{2}$$

where i_d and v_d are the direct current [A] and voltage [V] , and i_q and v_q are the quadrature current [A] and voltage [V], respectively. Via DQ transformation (2), the PM stepper motor dynamics (1) are changed into

$$\begin{aligned}\dot{\theta} &= \omega \\ \dot{\omega} &= \frac{1}{J}[-K_m i_q - B\omega - \tau_l] \\ \dot{i}_d &= \frac{1}{L}[v_d - Ri_d + N_r L\omega i_q] \\ \dot{i}_q &= \frac{1}{L}[v_q - Ri_q - N_r L\omega i_d - K_m\omega].\end{aligned} \tag{3}$$

As shown in (3), using DQ transformation makes PM stepper motor dynamics become simple so that it is more convenience to design the controller. In PM stepper motor dynamics (3), since the high frequency terms, i.e, $\sin(N_r\theta)$ and $\cos(N_r\theta)$ are removed, the stiff electrical dynamics become embedded and thus disappear in the PM stepper motor dynamics. However, the actual currents and voltages are not i_d, i_q, v_d and v_q but i_a, i_b, v_a and v_b. Removing the high frequency terms in (3) does not mean that the high frequency terms are actually rejected. Thus the effect of the stiffness of the electrical dynamics to the position control should be analyzed.

Generally, the microstepping method has been widely used for the position tracking. The key point of the microstepping method is to guarantee the desired currents i_{a_d} and i_{b_d} are defined as

$$i_{a_d} = \frac{V_{\max}}{R}\cos(N_r\theta_d),\ i_{b_d} = \frac{V_{\max}}{R}\sin(N_r\theta_d) \tag{4}$$

where θ_d is the desired position and $V_{\max}$ is the amplitude of the input. In order to guarantee the desired currents, several nonlinear control methods were proposed in [13–16]. In the PM stepper motor, the current dynamics are much faster than the mechanical dynamics. Therefore, although the microstepping control method guarantees the desired currents, the position tracking error appears in the position tracking during the nonzero velocity period [15]. To overcome these problem in the position tracking, various control methods that consist of the mechanical controller for the position tracking and the electrical controller for the current tracking have been developed in [19–30,32,33]. In these methods, both position and current tracking performances are important for the position tracking. In the position tracking control of PM stepper motor, since the electrical dynamics are stiff, the required bandwidth of the electrical dynamics for the current tracking is much wider than that of the mechanical dynamics for the position tracking. That is, the frequencies of the desired currents are much higher than the those of the desired position.

Table 1
PM stepper motor parameters.

Parameter	Value	Parameter	Value
L	0.0148 H	R	4.5 Ω
J	3×10^{-5} Kg · m^2	K_m	0.88 N · m/A
B	1×10^{-4} N · m · s/rad	N_r	50

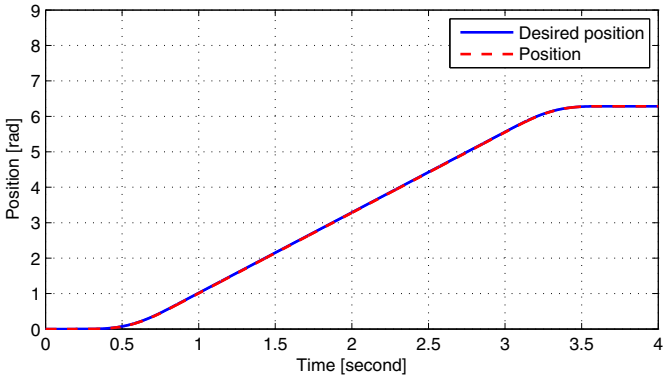

Fig. 1. The Desired position and the position of open-loop microstepping.

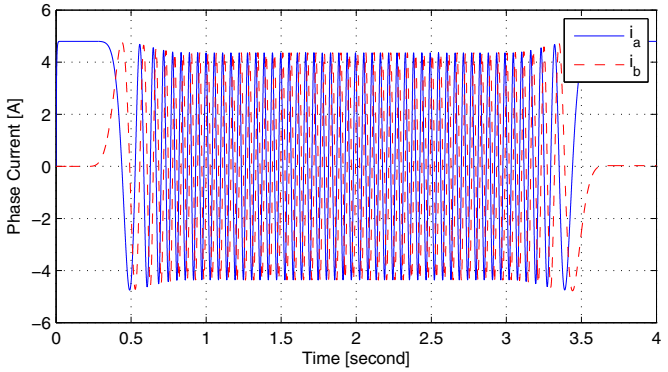

Fig. 2. i_a and i_b in open-loop microstepping.

The stiffness of the electrical dynamics will be demonstrated via simulations. We used the PM stepper motor parameters listed in Table 1 for simulations. The desired position shown in Fig. 1 was used in these simulations. In order to track the desired position, we use open-loop microstepping [14]

$$\begin{aligned}v_a &= V_{\max}\cos(N_r\theta_d) \\ v_b &= V_{\max}\sin(N_r\theta_d)\end{aligned} \tag{5}$$

where θ_d is the desired position and $V_{\max} = 24$ is the amplitude of the input voltage. In this simulation, $\tau_l = 0$. The position and currents of PM stepper motor of open-loop microstepping are shown in Figs. 1 and 2. We see that the frequencies of i_a and i_b is much higher than the frequencies of the position. High-bandwidth control methods have been designed to track both desired currents and position in much of the literature [19–30,32,33]. Actually, in the PM stepper motor, the available input to track both desired currents and position is bounded. The high-bandwidth control effort for the desired currents with high frequencies may require the significant portion of whole available input. Furthermore, although

the currents converge to the desired currents, it takes time for the position to converge to the desired position since the mechanical dynamics is much slower than the electrical dynamics. When the aim of the control in the PM stepper motor is the torque control, the whole available input can be used for the current control. However, in this paper, the main goal of the PM stepper motor is the position control, the whole available input cannot be used for only current control. The high-bandwidth control effort for the current tracking may cause the limitation of increasing the control gain in the position controller since the control effort for the current tracking may saturate the input voltages in the PM stepper motor. Thus, the high-bandwidth control for the current tracking may sacrifice the position tracking performance, especially during the acceleration and deceleration periods if the high-bandwidth control for the current tracking occupies the large portion of whole available input.

3. Singular perturbation model

General standard full singular perturbed system [34,35] is in the form of

$$\begin{aligned} \dot{x} &= f(t, x, z, \epsilon) \\ \epsilon \dot{z} &= g(t, x, z, \epsilon) \end{aligned} \tag{6}$$

where f and g are continuously differentiable and $x \in \mathbb{R}^n$ is the state of the slow subsystem, $z \in \mathbb{R}^m$ is the state of the fast subsystem, and ϵ is a small positive parameter. We use $x(t, \epsilon)$ and $z(t, \epsilon)$ to denote the solution of the full singular perturbation problem. The main idea of singular perturbation method is to divide the dynamics of the system into two separate time-scales, so that the resulting design problem is easier to solve than the design problem of the full singularly perturbed system [34,35]. It is assumed that $0 = g(t, x, z, 0)$ has isolated real roots

$$\bar{z} = h(t, x). \tag{7}$$

The reduced-order system is defined as

$$\dot{x} = f(t, x, h(t, x), 0). \tag{8}$$

$\bar{x}(t)$ is the solution of (8). And the quasi-steady-state is

$$\bar{z}(t) = h(t, \bar{x}(t)). \tag{9}$$

In order to shift the quasi-steady-state of z to the origin, we define y as

$$y = z - h(t, x). \tag{10}$$

With new time variable $\frac{d\tau}{dt} = \frac{1}{\epsilon}$, the boundary-layer system is obtained as

$$\frac{dy}{d\tau} = g(t, x, y + h(t, x), 0) \tag{11}$$

where t and x are treated as fixed parameters. From Theorem 11.2 in [35], we conclude that if the boundary-layer model (11) is exponentially stable and the reduced-order system (8) is also exponentially stable, then there exists a positive constant ϵ^* such that for $0 < \epsilon < \epsilon^*$, the system (6) has a unique solution $x(t, \epsilon)$, $z(t, \epsilon)$ on $[t_0, \infty)$, and $x(t, \epsilon) - \bar{x}(t) = O(\epsilon)$ where the definition of the letter 'O' is introduced in [38]. Moreover, given any $t_b > t_0$, there exists $0 < \epsilon < \epsilon^*$ such that $z(t, \epsilon) - h(t, \bar{x}) = O(\epsilon)$ holds uniformly for $t \in [t_b, \infty)$.

In practically all well designed PM stepper motors, L can play the role of the parameter ϵ [35]. Therefore, the PM stepper motor (1) can be rewritten as

$$\begin{aligned} \dot{\theta} &= \omega \\ \dot{\omega} &= \frac{1}{J}[-K_m i_a \sin(N_r\theta) + K_m i_b \cos(N_r\theta) - B\omega - \tau_l] \\ \epsilon \dot{i}_a &= v_a - R i_a + K_m \omega \sin(N_r\theta) \\ \epsilon \dot{i}_b &= v_b - R i_b - K_m \omega \cos(N_r\theta) \end{aligned} \tag{12}$$

where $\epsilon = L$. In PM stepper motor (12), the electrical dynamics are fast dynamics and the mechanical dynamics are slow dynamics. Therefore, we can use singular perturbation theory to solve the position tracking problem. The voltage inputs are designed as the function of state variables. Thus, the PM stepper motor (12) can be rewritten in the form of a singular perturbation model as follows

$$\begin{aligned} \dot{x} &= f(t, x, i_a, i_b) \\ \epsilon \dot{i}_a &= g_a(t, x, i_a, \epsilon) \\ \epsilon \dot{i}_b &= g_b(t, x, i_b, \epsilon) \end{aligned} \tag{13}$$

where $x = [\theta, \omega]^T$. We define $\bar{i}_a$ and $\bar{i}_b$ as

$$\begin{aligned} \bar{i}_a &= \frac{v_a + K_m \omega \sin(N_r\theta)}{R} = h_a(t, v_a, x), \\ \bar{i}_b &= \frac{v_b - K_m \omega \cos(N_r\theta)}{R} = h_b(t, v_b, x). \end{aligned} \tag{14}$$

Lemma 1. *Consider the singular perturbation problem of PM stepper motor (1). The origin of the boundary-layer model in (12) is exponentially stable.* ◊

Proof. To move the equilibrium point to the origin, let us define y_a and y_b as

$$\begin{aligned} y_a &= i_a - h_a(t, v_a, x) \\ y_b &= i_b - h_b(t, v_b, x). \end{aligned} \tag{15}$$

Differentiating and multiplying ϵ on both sides of (15) results in

$$\begin{aligned} \epsilon \dot{y}_a &= \epsilon \dot{i}_a - \epsilon \dot{h}_a \\ \epsilon \dot{y}_b &= \epsilon \dot{i}_b - \epsilon \dot{h}_b. \end{aligned} \tag{16}$$

With new time variable $\frac{d\tau}{dt} = \frac{1}{\epsilon}$, the boundary-layer system is obtained as

$$\begin{aligned} \frac{dy_a}{d\tau} &= g_a(t, x, y_a + h_a, 0) \\ &= v_a - R\left(y_a + \frac{v_a + K_m \omega \sin(N_r\theta)}{R}\right) + K_m \omega \sin(N_r\theta) \\ &= -R y_a, \\ \frac{dy_b}{d\tau} &= g_b(t, x, y_b + h_b, 0) \\ &= v_b - R\left(y_b + \frac{v_b - K_m \omega \cos(N_r\theta)}{R}\right) - K_m \omega \cos(N_r\theta) \\ &= -R y_b. \end{aligned} \tag{17}$$

Since R is always positive, the origin of boundary-layer system (17) is exponentially stable. Furthermore, the region of attraction of the fast manifold covers the whole domain. □

From Theorem 3.1 in [34], the eigenvalues of the fast dynamics can be approximated as

$$\begin{aligned} \lambda_a &= \frac{-R + O(\epsilon)}{\epsilon} \\ \lambda_b &= \frac{-R + O(\epsilon)}{\epsilon}. \end{aligned} \tag{18}$$

Therefore, as the resistance R is bigger and the inductance $L = \epsilon$ is smaller, the fast dynamics play a small role in the transient response. Thus, a bigger resistance or a smaller inductance is expected. This limits the use of singular perturbation theory to solve PM stepper motor applications. Although there is limit mentioned above, since L is small in practically all well-designed PM stepper motors [35], this theory can be used. Eqs. (17) and (18) shows that only passive term $-Ri_a$ and $-Ri_b$ is enough for the current tracking if L is small in practically all well-designed PM stepper motors. The reduced-order model can be obtained as

$$J\ddot{\theta} = \bar{\tau} - B\dot{\theta} - \tau_l \tag{19}$$

where $\bar{\tau} = -K_m\bar{i}_a \sin(N_r\theta) + K_m\bar{i}_b \cos(N_r\theta)$.

4. Controller design

The position tracking error e_1 is defined as

$$e_1 = \theta - \theta_d \tag{20}$$

where θ_d is the desired position. And let us define e_2 as

$$e_2 = \dot{e}_1 + k_{1_p} e_1 \tag{21}$$

where k_1 is a positive constant. We define the integration of the position tracking error as

$$e_0 = \int_0^t (\theta - \theta_d) d\tau. \tag{22}$$

The integrator is added to the controller to eliminate any steady-state error due to constant disturbances. From (19), (20), (21), and (22) the reduced-order model becomes

$$\begin{aligned} &J(\dot{e}_2 + k_0 e_0 + k_1 e_1 + k_2 e_2) \\ &\quad = \bar{\tau} - B\dot{\theta} - \tau_l - J(\ddot{\theta}_d - k_{1_p}\dot{e}_1 - k_0 e_0 - k_1 e_1 - k_2 e_2) \end{aligned} \tag{23}$$

where k_2 is a positive constant. We define τ_d as

$$\tau_d = B\dot{\theta} + \tau_l + J(\ddot{\theta}_d - k_{1_p}\dot{e}_1 - k_0 e_0 - k_1 e_1 - k_2 e_2). \tag{24}$$

Then, (23) becomes

$$J(\dot{e}_2 + k_0 e_0 + k_1 e_1 + k_2 e_2) = \bar{\tau} - \tau_d. \tag{25}$$

The reduced-order model dynamics are given as

$$\underbrace{\begin{bmatrix} \dot{e}_0 \\ \dot{e}_1 \\ \dot{e}_2 \end{bmatrix}}_{\dot{e}} = \underbrace{\begin{bmatrix} 0 & 1 & 0 \\ 0 & -k_{1_p} & 1 \\ -k_0 & -k_1 & -k_2 \end{bmatrix}}_{A} \underbrace{\begin{bmatrix} e_0 \\ e_1 \\ e_2 \end{bmatrix}}_{e} + \begin{bmatrix} 0 \\ 0 \\ \frac{1}{J} \end{bmatrix} (\bar{\tau} - \tau_d) \tag{26}$$

In order to design the control law, we use the commutation scheme proposed in [33] such as

$$\begin{aligned} i_{a_d} &= -\frac{\tau_d}{K_m} \sin(N_r\theta) \\ i_{b_d} &= \frac{\tau_d}{K_m} \cos(N_r\theta). \end{aligned} \tag{27}$$

Then the voltage inputs are

$$\begin{aligned} v_a &= Ri_{a_d} - K_m\omega \sin(N_r\theta) \\ v_b &= Ri_{b_d} + K_m\omega \cos(N_r\theta). \end{aligned} \tag{28}$$

Lemma 2. *For the singular perturbed system (13), if f, g_a, g_b and their partial derivatives are sufficiently smooth functions and both the reduced-order system and the boundary-layer system are exponentially stable on a compact set, then there exists ϵ^* such that for all $0 < \epsilon < \epsilon^*$, the system (13) is exponentially stable at the equilibrium point (for proof, see Theorem in 11.4 [35]).* ◊

Theorem 1. *Consider the singular perturbation problem of PM stepper motor (1). Suppose that the control law (27) and (28) is used in PM stepper motor. If k_{1_p}, k_0, k_1, and k_2 are designed such that the matrix A is Hurwitz, then there exists a positive constant ϵ^* such that for $0 < \epsilon < \epsilon^*$ the tracking error e decays exponentially.* ◊

Proof. From (14), (28),

$$\begin{aligned} \bar{i}_a &= i_{a_d} = h_a(t, \bar{x}) \\ \bar{i}_b &= i_{b_d} = h_b(t, \bar{x}). \end{aligned} \tag{29}$$

In Lemma 1, it was shown that the origin of the boundary-layer model in (12) is exponentially stable. Therefore, i_a and i_b exponentially converge to quasi-steady-state i_{a_d} and i_{b_d}. Since the control law (27) and (28) is used, the reduced-order model (25) becomes

$$J(\dot{e}_2 + k_0 e_0 + k_1 e_1 + k_2 e_2) = 0. \tag{30}$$

Thus, The reduced-order model dynamics (26) become

$$\dot{e} = Ae \tag{31}$$

Therefore, e exponentially converges to zero if k_{1_p}, k_0, k_1, and k_2 are designed such that the matrix A is Hurwitz. Finally, we conclude that the origins of the boundary-layer model and the reduced-order model are exponentially stable. Therefore, using Theorem 11.4 in [35], there exists a positive constant ϵ^* such that for $0 < \epsilon < \epsilon^*$ the tracking error e decays exponentially. □

Since the position tracking error is of the order $O(\epsilon) = O(L)$ during the non-zero velocity period when the desired position θ_d has a dynamic profile, it is clear that a system with sufficiently small inductance tracks a desired position with very small error and the position tracking performance depends on L. In the final position, the position tracking error becomes zero. As commented in Lemma 2, from Theorem 11.4 in [35] there exists a upper limit L^* of the inductance such that if $L < L^*$, then the closed-loop stability is guaranteed although it is very difficult to numerically obtain this upper limit. Generally, this upper limit is usually much larger than the normal range of the inductance encountered in practical applications. Using singular perturbation method gives us the benefit. We do not need to consider the uncertainty of the inductance, which often happens in the manufacturing process. Hence, the controller using singular perturbation method is robust to the uncertainty of the inductance. That is, the stability of the closed-loop is guaranteed under the uncertainty of the inductance.

The block diagram of the proposed method is shown in Fig. 3. The proposed method consists of the mechanical controller (position controller), the commutation scheme, and the electrical controller (current controller) The desired torque τ_d for the position tacking is derived by the mechanical controller (24). Then the desired currents i_{a_d} and i_{b_d} to generate τ_d are derived by the commutation scheme (27). Finally, the input voltages v_a and v_b (28) are given to the PM stepper motor by the electrical controller. In summary, the proposed method, STMMS, designed using singular

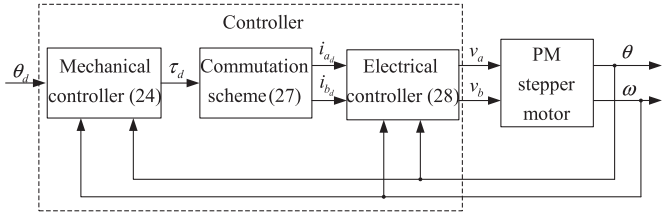

Fig. 3. Block diagram of the proposed method.

perturbation theory is

$$
\begin{aligned}
e_2 &= \dot{e}_1 + k_{1_p} e_1 \\
\tau_d &= B\dot{\theta} + \tau_l + J(\ddot{\theta}_d - k_{1_p}\dot{e}_1 - k_0 e_0 - k_1 e_1 - k_2 e_2) \\
i_{a_d} &= -\frac{\tau_d}{K_m}\sin(N_r\theta) \\
i_{b_d} &= \frac{\tau_d}{K_m}\cos(N_r\theta) \\
v_a &= Ri_{a_d} - K_m\omega\sin(N_r\theta) \\
v_b &= Ri_{b_d} + K_m\omega\cos(N_r\theta).
\end{aligned} \tag{32}
$$

Since the current tracking controller (28) in (32) consists of the feedforward part and the back-emf cancellation part, the proposed method (32) does not require current feedback for the current tracking although the proposed method is not an observer-based method.

5. Simulation and experimental results

The performance of STMMS was evaluated with simulations and experiments. The reference position shown in Fig. 1 and $\tau_l = 0.1$ were used. The PM stepper motor parameters listed in Table 1 were used for simulations and experiments. To evaluate the effect of the wide bandwidth control effort for the current tracking to the position tracking performance, we used two algorithms: the proposed STMMS and the FOC proposed in [32]. The FOC was designed for the position tracking with the high current tracking performances. Thus, instead of the current tracking controller (28), the following current tracking controller using high control gain and current feedback was used

$$
\begin{aligned}
v_a &= (Ri_a - K_m\omega\sin(N_r\theta)) + L(\dot{i}_{a_d} + \rho(i_{a_d} - i_a)) \\
v_b &= (Ri_b + K_m\omega\cos(N_r\theta)) + L(\dot{i}_{b_d} + \rho(i_{b_d} - i_b))
\end{aligned} \tag{33}
$$

where ρ is the current tracking control gain. For fair comparison, the FOC used the same mechanical controller (24) and the commutation scheme (27).

The block diagram of the proposed method is shown in Fig. 4. The FOC is implemented as follows:

$$
\begin{aligned}
e_2 &= \dot{e}_1 + k_1 e_1 \\
\tau_d &= B\dot{\theta} + \tau_l + J(\ddot{\theta}_d - k_{1_p}\dot{e}_1 - k_0 e_0 - k_1 e_1 - k_2 e_2) \\
i_{a_d} &= -\frac{\tau_d}{K_m}\sin(N_r\theta) \\
i_{b_d} &= \frac{\tau_d}{K_m}\cos(N_r\theta) \\
v_a &= (Ri_a - K_m\omega\sin(N_r\theta)) + L(\dot{i}_{a_d} + \rho(i_{a_d} - i_a)) \\
v_b &= (Ri_b + K_m\omega\cos(N_r\theta)) + L(\dot{i}_{b_d} + \rho(i_{b_d} - i_b)).
\end{aligned} \tag{34}
$$

The main differences between the STMMS (32) and the FOC (34) are the current feedback and high gain ρ used in the FOC (34) for the high current tracking performance. In the FOC (33), Ri_a and Ri_b are used to cancel the passive term Ri_a and Ri_b. For the perfect current tracking, $L\dot{i}_{a_d}$ is used. On the other hand, Ri_{a_d} and Ri_{b_d} are utilized for the use of the passive term Ri_a and Ri_b for the current tracking in the proposed method (27). Since the FOC required high gain ρ for the current tracking, the STMMS and the FOC used different control gains with the consideration of the input voltage saturation. In the STMMS, $k_{1_p} = 40000$, $k_0 = 10$, $k_1 = 20$, and $k_2 = 100$. With the input voltage saturation, the control gains k_1 and k_2 in the FOC (34) were relatively lower than those in the STMMS (32) due to the control effort to track the desired currents in the FOC (34). We performed the FOC for two different cases:

- Case 1: $k_{1_p} = 1000$, $k_0 = 10$, $k_1 = 20$, $k_2 = 100$, and $\rho = 25{,}000$
- Case 2: $k_{1_p} = 10{,}000$, $k_0 = 10$, $k_1 = 20$, $k_2 = 100$, and $\rho = 10{,}000$.

In Case 1, the control gains were chosen to obtain small steady-state position tracking error during the constant velocity period while keeping good current tracking. In Case 2, different control gains were selected to improve transient response during the acceleration and deceleration periods. Since Ri_a and Ri_b are used to cancel the passive term Ri_a and Ri_b in the FOC (34), the control gain should be large enough for the current tracking.

5.1. Simulation results

Fig. 5 shows the position tracking errors of the FOC (Cases 1 and 2) and the STMMS. Since the large electrical control gain $\rho = 25{,}000$ for the wide bandwidth control, and the small mechanical control gains $k_{1_p} = 1000$, $k_0 = 10$, $k_1 = 20$, and $k_2 = 100$ were used in the FOCs (Case 1), the overshoots in the position tracking error appeared during the acceleration and deceleration periods. In the FOC (Case 2), the relatively small electrical control

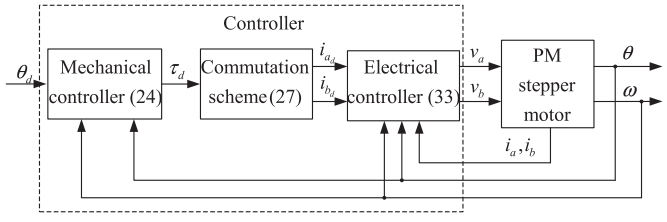

Fig. 4. Block diagram of the FOC.

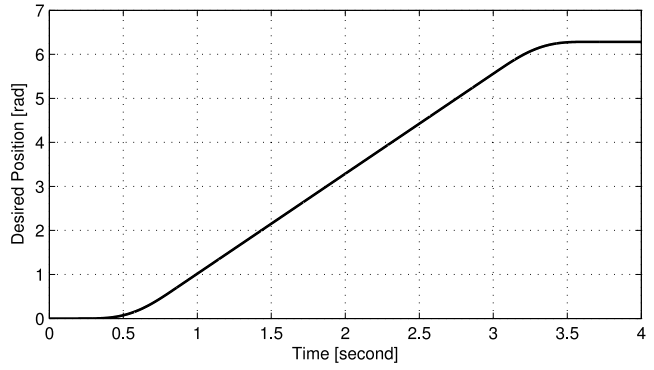

(a) Desired position (θ_d)

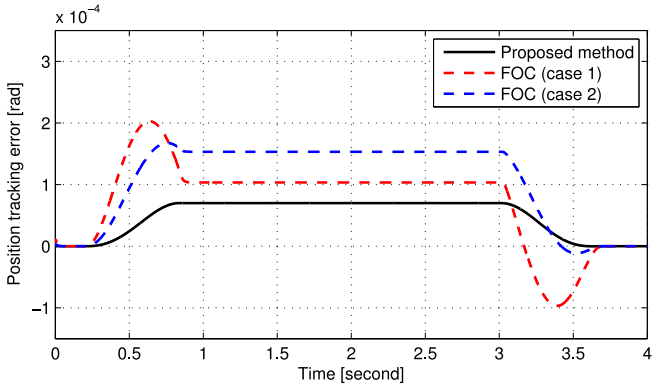

(b) Position tracking errors of the FOCs and the STMMS ($\theta_d - \theta$)

Fig. 5. Position tracking performance of the FOCs and the STMMS.

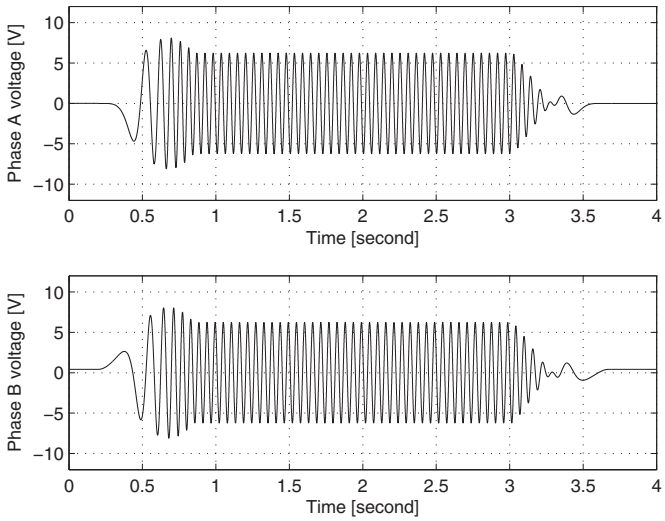

(a) FOC (case 1)

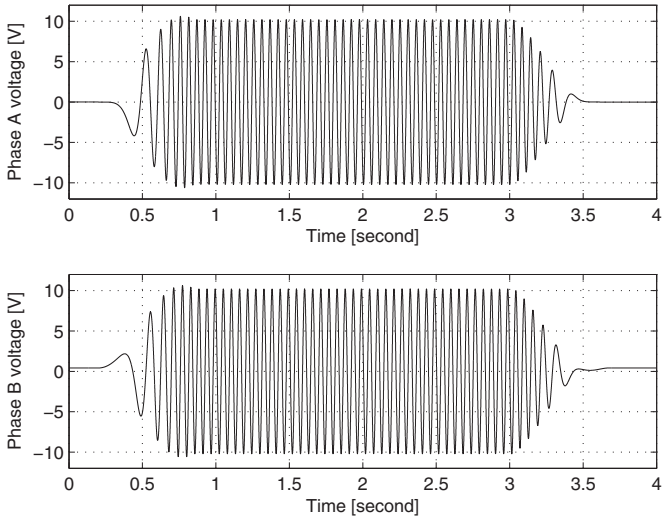

(b) FOC (case 2)

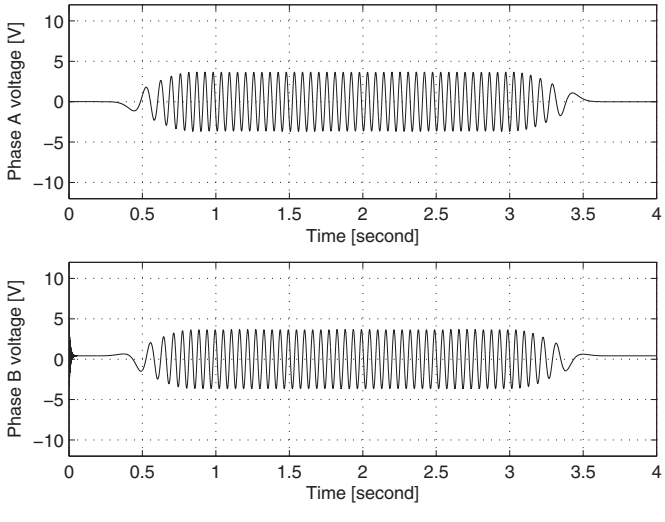

(c) STMMS

Fig. 6. Input voltages of the FOCs and the STMMS (v_a and v_b).

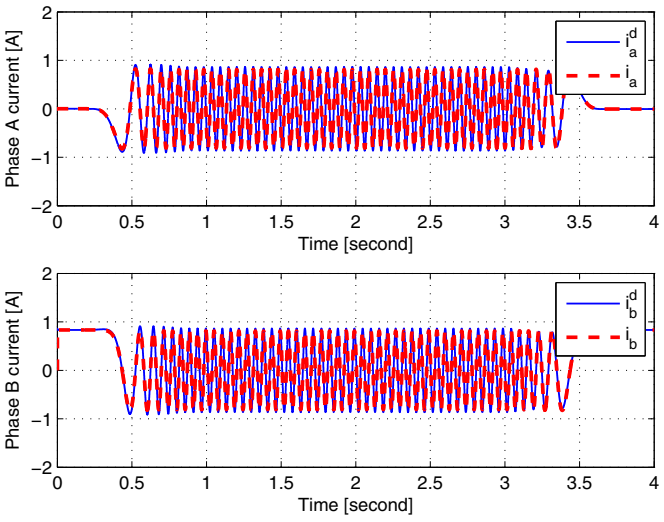

(a) FOC (case 1)

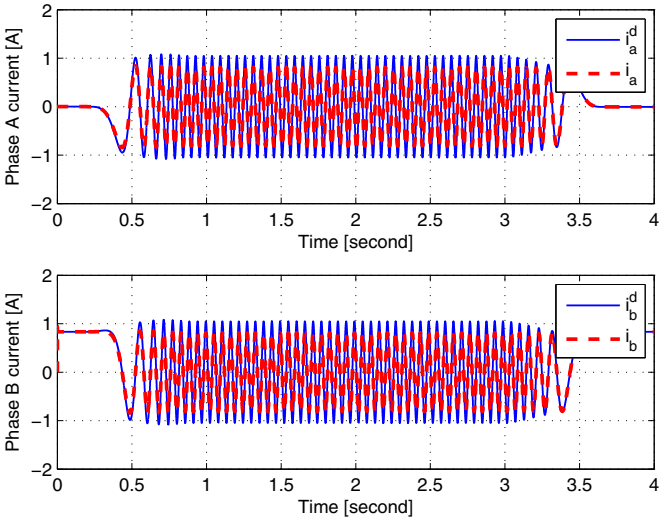

(b) FOC (case 2)

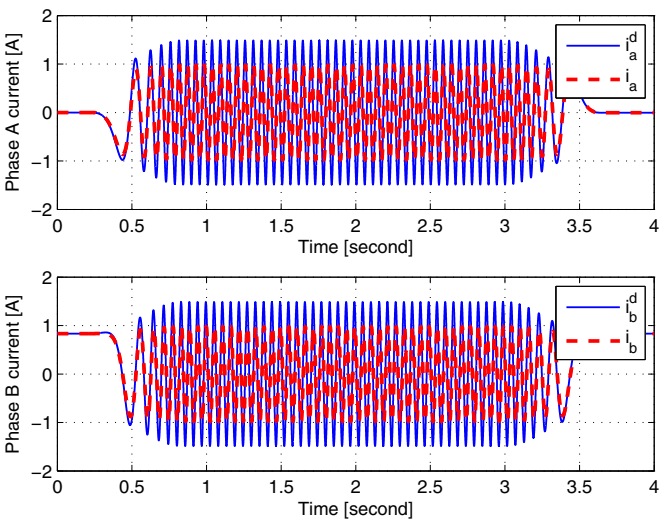

(c) STMMS

Fig. 7. Current tracking performances of the FOCs and the STMMS (i_a and i_b).

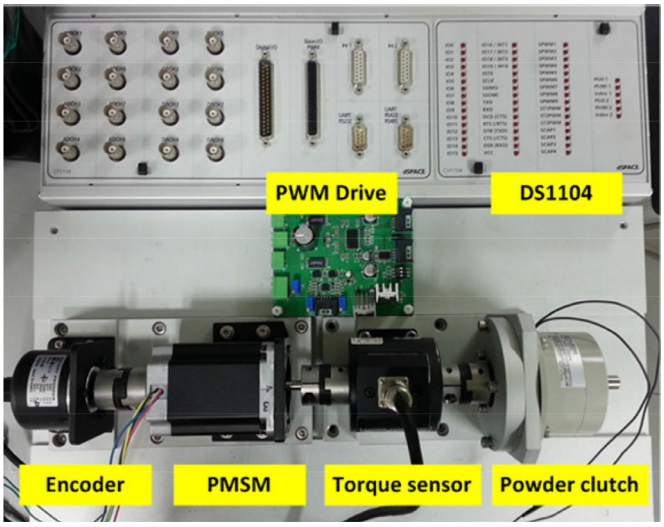

Fig. 8. Photograph of the experimental setup.

gain $\rho = 10{,}000$, and the relatively large mechanical control gains $k_{1_p} = 10{,}000$, $k_0 = 10$, $k_1 = 20$, and $k_2 = 100$ were used compared with those of the FOC (Case 1). In the FOC (Case 2), the larger position control gain gave us the improvement of the position tracking performance during the transient response. Note that the FOC was designed by using Lyapunov method for both position and current tracking. Thus, the current tracking performance is also important. Consequently, although the FOC (Case 2) used the larger position control gain with the lower current control gain compared to the FOC (Case 1), the FOC (Case 2) had the larger position tracking error during constant velocity periods.

Fig. 6 shows the input voltages of the FOC (Cases 1 and 2) and the STMMS. The input voltages of FOC (Cases 1 and 2) were larger than those of STMMS due to the high control gains, $\rho = 25{,}000$ and $\rho = 10{,}000$ for the high current tracking performance. In Case 2, the high mechanical control gain $k_{1_p} = 10{,}000$ with the high electrical control gain $\rho = 10{,}000$ resulted in the largest input voltages. On the other hand, the STMMS had the smallest input voltages since the high electrical control gain part was not used. Furthermore, the position tracking error of the STMMS was the smallest among three cases although wide bandwidth control was not used in the STMMS. The proposed method had the position tracking error that is of the order $O(\epsilon) = O(L)$ so that the position tracking error was not zero but it was zero in the final position (3.5–4.0 s).

Fig. 7 shows the current tracking performances of three cases. We see that the FOC (Case 1) had the best current tracking performance. However, the control effort required to maintain a wide bandwidth in the FOC sacrificed the position tracking performance during the acceleration and deceleration periods as shown in Fig. 5. In the FOC (Case 2) and the STMMS, the poor current tracking performances increased the desired currents during the constant velocity period. The STMMS had the poor current tracking performance since the STMMS did not use the high gain in the current-loop to avoid the degradation of the position tracking performance. Despite the poor current tracking performance, the STMMS had the best position tracking performance. Figs. 5 and 7 show that the high performance in the current tracking does not necessarily entail high performance in the position tracking.

5.2. Experiment results

Experiments were executed to evaluate the performances of the proposed method. The photo of the experimental setup is shown in Fig. 8. The model of PM stepper motor is PK268-02B, which is a two-phase PM stepper motor manufactured by Orientalmotor Co. The PWM driver, DRV8412 from Texas Instruments Co., was used where the PWM switching frequency was 50 kHz. The powder clutch, ZKG-20AN from MITSUBISHI, was used to generate the load torque. An incremental optical encoder (8000 pulse/rev) was used for the position feedback and quadrature signals were used to obtain × 4 resolution (32,000 pulse/rev). DS1104 manufactured by dSPACE Inc. was used as an embedded real-time controller. The control sampling rate was 5 kHz.

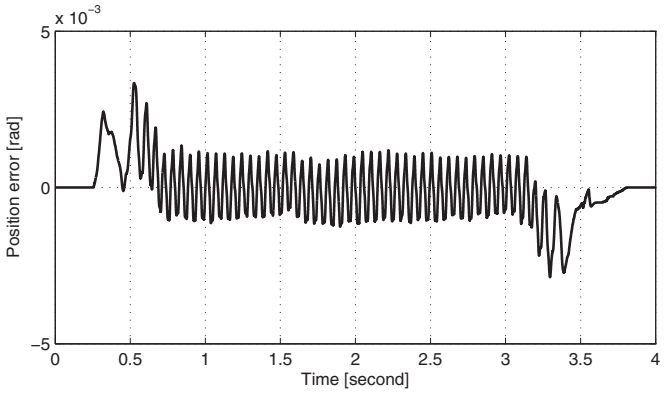

(a) FOC (case 1)

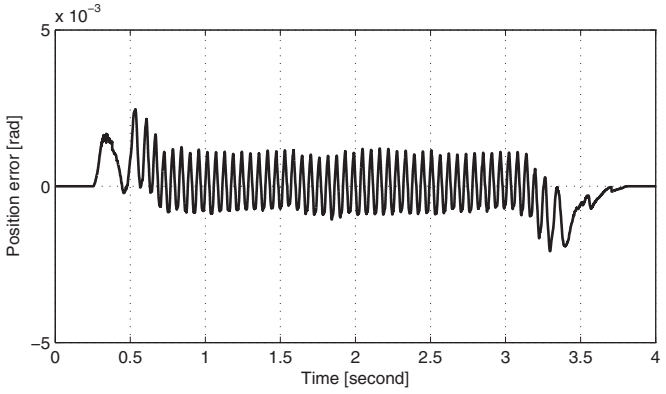

(b) FOC (case 2)

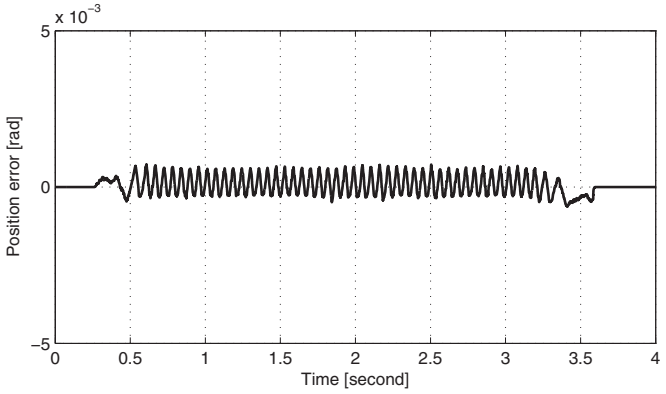

(c) STMMS

Fig. 9. Position tracking errors of the FOCs and the STMMS ($\theta_d - \theta$).

The position tracking errors of three methods are shown in Fig. 9. Due to the high gain in the current controller, the FOC (Case 1) had the largest overshoot and ripple among three methods. The

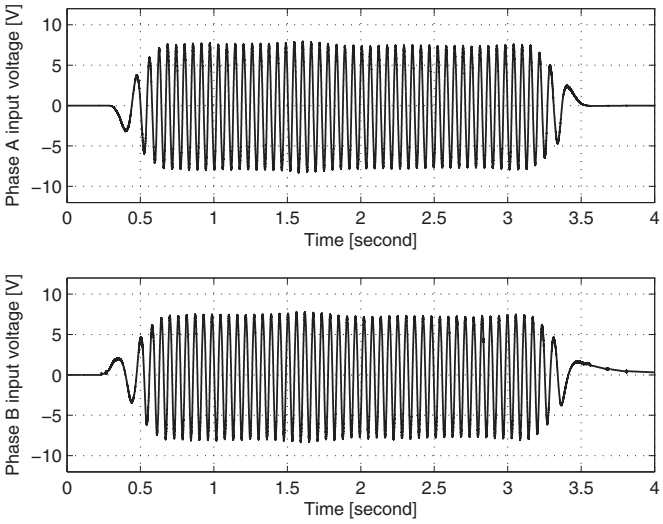

(a) FOC (case 1)

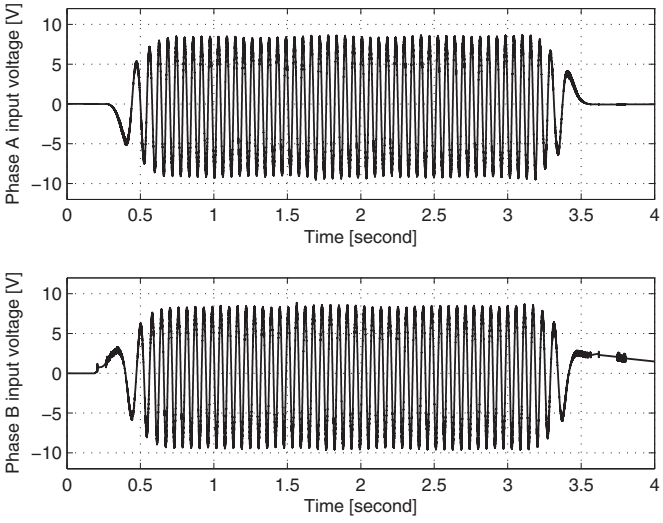

(b) FOC (case 2)

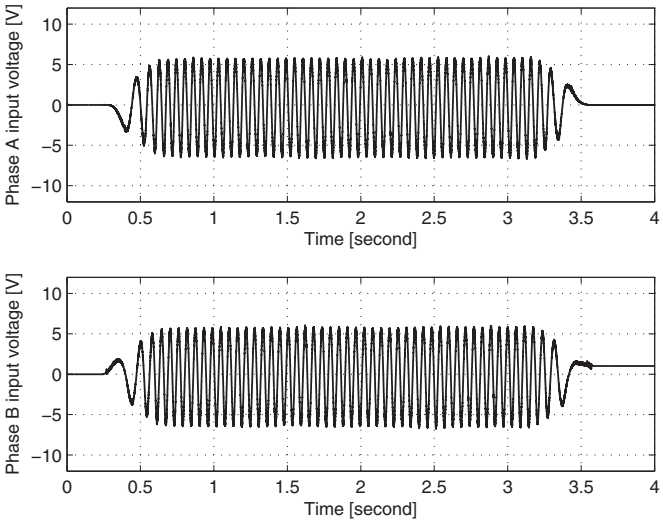

(c) STMMS

Fig. 10. Input voltages of the FOCs and the STMMS (v_a and v_b).

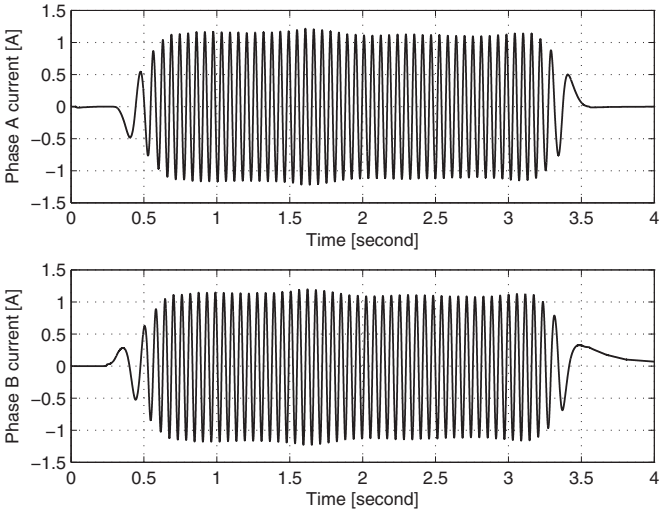

(a) FOC (case 1)

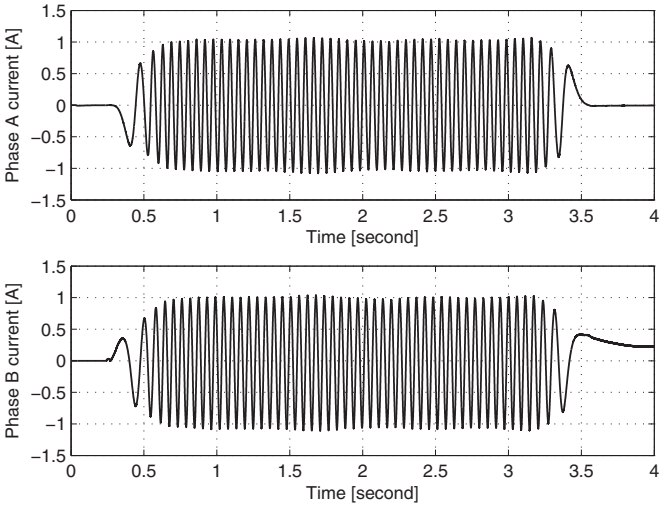

(b) FOC (case 2)

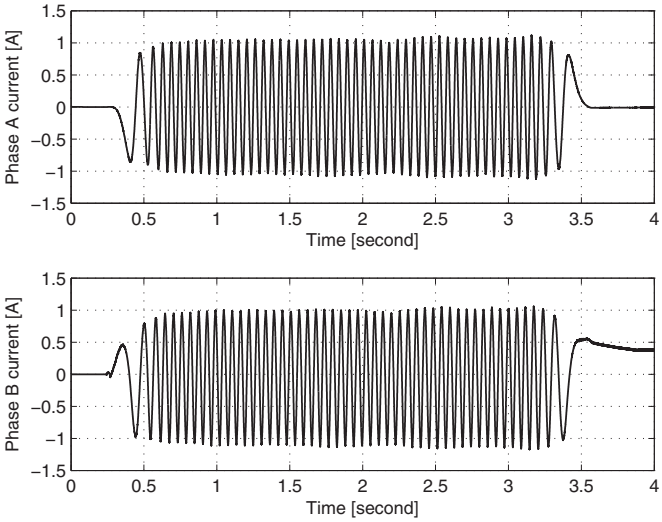

(c) STMMS

Fig. 11. Currents of the FOCs and the STMMS (i_a and i_b).

FOC (Case 2) with the relative lower gain in the current controller had the smaller overshoot and ripple than the FOC (Case 1). However, the FOC (Case 2) still had the overshoot during the acceleration and deceleration periods and the relatively large ripple during the constant period. The STMMS had the reduced overshoot in the position compared to the FOCs (Cases 1 and 2.) The position ripples not observed in Fig. 5 appeared in experiments. These ripples are unavoidable due to quantization effect, PWM driver switching noise, encoder coupling effect, modeling and parameter uncertainties, nonideal sinusoidal flux distribution, and torque ripple's harmonics. The frequency of the main component in the ripples was $N_r\omega$ from the torque ripple. From (26), the sensitivity function from the torque error $\tilde{\tau} = \bar{\tau} - \tau_d$ to the position error $e_1(t)$ is obtained as

$$\frac{E_1(s)}{\tilde{T}(s)} = \frac{1}{J}\frac{s}{s^3 + (k_2 + k_{1p})s^2 + (k_1 + k_{1p}k_2)s + k_0} \tag{35}$$

where $E_1(s)$ and $\tilde{T}(s)$ are the Laplace transforms of $e_1(t)$ and $\tilde{\tau}$, respectively. From (35), the position ripples can be reduced more as the position control gain gets higher. Thus the FOC of the Case 2 reduced the ripples more than the FOC of the Case 1 since the FOC of the Case 2 had the higher position control gain compared to the FOC of the Case 1. Since the STMMS had the highest position control gain, the best reduction of the position ripples was observed in the STMMS. Note that the position tracking error was covered with the ripple since the position ripple was relatively large compared to the position tracking error during constant velocity period.

Figs. 10 and 11 show the input voltages and the currents of three methods. Due to the PWM driver, parameter uncertainties, the experimental input voltages and currents slightly became different compared to the simulation input voltages. Since the control effort to maintain a wide bandwidth was not used in the STMMS, the input voltages in the STMMS were smaller than those in the FOCs (Cases 1 and 2). The currents of the FOC (Case 2) were slightly smaller than that of the FOC (Case 1) since the FOC (Case 2) did not use the high gain in the electrical controller. From the experimental results, it is shown that the STMMS improved the position tracking performance without large input voltages inputs for the high current tracking performance.

6. Conclusion

The STMMS based on singular perturbation theory was proposed to improve the position tracking performance of PM stepper motors. The torque modulated microstepping method was applied with a simplified current tracking control. Using applied conditions and stability proofs, we found that the proposed control design procedure is simplified from singular perturbed system analysis. The main advantage of the proposed STMMS is that the improved transient response and reduced ripples in the position control are achieved without a wide bandwidth control effort by the STMMS. The STMMS does not use current feedback for the current tracking. Furthermore, the STMMS guarantees the stability under the inductance uncertainty in the position tracking. Via simulations and experiments, we validated that the STMMS reduced not only overshoot but also position ripples although wide bandwidth control was not used in the STMMS. The STMMS used the voltages less than the previous method.

Acknowledgment

This research was supported by Basic Science Research Program through the National Research Foundation of Korea (NRF) funded by the Ministry of Education (no. 2013007682).

References

[1] Kenjo T. Stepping motors and their microprocessor control. New York: Clarendon; 1984.
[2] Siripala PJ, Sekercioglu YA. A generalised solution for generating stepper motor speed profiles in real time. Mechatronics 2013;23(5):541–7.
[3] Bodson M, Sato JS, Silver SR. Spontaneous speed reversals in stepper motors. IEEE Trans Control Syst Technol 2006;14(2):369–73.
[4] Jones DW. Control of stepping motors, handbook of small electric motors. New York: McGraw-Hill; 2001.
[5] Carrica D, Funes MS, González SA. Novel stepper motor controller based on FPGA hardware implementation. IEEE/ASME Trans Mechatron 2003;8(1):120–4.
[6] STMicroelectronics, stepper motor - two-phase bipolar stepper motors. Available online at: http://www.st.com/web/en/catalog/apps/SE413/AS382/AC906.
[7] Moon S, Kim DH. Step-out detection and error compensation for a microstepper motor using current feedback. Mechatronics 2014;24(3):265–73.
[8] Kang BJ, Liaw CM. A robust hysteresis current-controlled PWM inverter for linear PMSM driven magnetic suspended positioning system. IEEE Trans Ind Electron 2001;48(5):956–67.
[9] Orientalmotor, basics of motion control. Available online at: http://www.orientalmotor.com/products/ac-dc-step-motors/alphastep-overview.html.
[10] Sanyo-denki, 2 phase stepping systems. Available online at: http://www.sanyo-denki.com/Data/Servo/catalogs/F2{_}ver1.pdf.
[11] Feng Z, Acarnley PP. Extrapolation technique for improving the effective resolution of position encoders in permanent-magnet motor drives. IEEE/ASME Trans Mechatron 2008;13(4):410–15.
[12] Tsui KWH, Cheung NC, Yuen KCW. Novel modeling and damping technique for hybrid stepper motor. IEEE Trans Ind Electron 2009;56(1):202–11.
[13] Ghafari AS, Behzad M. Investigation of the micro-step control positioning system performance affected by random input signals. Mechatronic 2005;15(10):1175–89.
[14] Kim W, Shin D, Chung CC. Lyapunov-based controller with a passive nonlinear observer to improve position tracking performance of microstepping in permanent magnet stepper motors. Automatica 2012;48(12):3064–74.
[15] Kim W, Shin D, Chung CC. Microstepping using a disturbance observer and a variable structure controller for permanent magnet stepper motors. IEEE Trans Ind Electron 2013a;60(7):2689–99.
[16] Shin D, Kim W, Lee Y, Chung CC. Phase compensated microstepping for permanent magnet stepper motors. IEEE Trans Ind Electron 2013;60(12):5773–5780.
[17] Kim W, Chung CC. Novel position detection method for permanent magnet stepper motors using only current feedback. IEEE Trans Magn 2011;47(10):3590–3.
[18] Henke B, Sawodny O, Schmidt S, Neumann R. Modeling of hybrid stepper motors for closed-loop operation. In: Proceedings of the sixth IFAC symposium mechatronic systems; 2013. p. 177–83.
[19] Zribi M, Chiasson J. Position control of a PM stepper motor by exact linearization. IEEE Trans Autom Control 1991;36(5):620–5.
[20] Bodson M, Chiasson J, Novotnak R, Rekowski R. High-performance nonlinear feedback control of a permanent magnet stepper motor. IEEE Trans Control Syst Technol 1993;1(1):5–14.
[21] Dawson D, Hu J, Burg T. Nonlinear control of electric machinery. Piscataway, NJ: IEEE Press; 1995.
[22] Marino R, Peresada S, Tomei P. Nonlinear adaptive control of permanent magnet step motors. Automatica 1995;31(11):1595–604.
[23] Khorrami F, Krishnamurthy P, Melkote H. Modeling and adaptive nonlinear control of electric motors. Heidelberg: Springer Verlag; 2003.
[24] Krishnamurthy P, Khorrami F. Voltage-fed permanent-magnet stepper motor control via position-only feedback. IEE Proc Control Theory Appl 2004;151(4):499–510.
[25] Chen WD, Yung KL, Cheng KW. A learning scheme for low-speed precision tracking control of hybrid stepping motors. IEEE/ASME Trans Mechatron 2006;11(3):265–362.
[26] Le QN, Jeon JW. Neural-network-based low-speed-damping controller for stepper motor with an FPGA. IEEE Trans Power Electron 2010;57(9):3167–3180.
[27] Bendjedia M, Ait-Amirat Y, Walther B, Berthon A. Position control of a sensorless stepper motor. IEEE Trans Power Electron 2012;27(2):578–87.
[28] Masi A, Butcher M, Martino M, Picatoste R. An application of the extended Kalman filter for a sensorless stepper motor drive working with long cables. IEEE Trans Power Electron 2012;59(11):4217–25.
[29] Corradini ML, Ippoliti G, Longhi S, Marchei D, Orlando G. A quasi-sliding mode observer-based controller for PMSM drives. Asian J Control 2013;15(2):380–390.
[30] Zaky MS, Ismaeil EM, Khater MM. Gain scheduling adaptive proportional-integral controller for a field-oriented control of hybrid stepper motor drives. Electr Power Compon Syst 2013;40(7):777–91.
[31] Sun X, Chen L, Yang Z, Zhu H. Speed-sensorless vector control of a bearingless induction motor with artificial neural network inverse speed observer.. IEEE/ASME Trans Mechatron 2013;18(4):1357–66.
[32] Kim W, Shin D, Chung CC. Microstepping with nonlinear torque modulation for permanent magnet stepper motors. IEEE Trans Control Syst Technol 2013b;21(5):1971–9.

[33] Kim W, Yang C, Chung CC. Design and implementation of simple field oriented control for permanent magnet stepper motors without DQ transformation. IEEE Trans Magn 2011;47(10):4231–4.
[34] Kokotovic P, Khalil H, O'Reilly J. Singular perturbation methods in control: Analysis and design. New York: Academic Press; 1991.Republished by SIAM.
[35] Khalil H. Nonlinear systems. 3rd. Upper Saddle River, NJ: Prentice-Hall; 2002.
[36] Chen JJ, Chin KP. Reduced-order control of permanent magnet synchronous motors. Proceedings of the IEEE annual conference on industrial electronics society; 1999. p. 1361–6.
[37] Chiasson J. Modeling and high-performance control of electric machines. Hoboken, NJ: Wiley-Interscience; 2005.
[38] Marsden JE, Hoffman MJ. Elementary classical analysis. Macmillan; 1993.